International Journal of Biological Macromolecules 156 (2020) 522–530

Contents lists available at ScienceDirect

International Journal of Biological Macromolecules

journal homepage: http://www.elsevier.com/locate/ijbiomac

Heat shock protein 90 kDa (Hsp90) from *Aedes aegypti* has an open conformation and is expressed under heat stress

Natália G. Quel [a], Glaucia M.S. Pinheiro [a], Luiz Fernando de C. Rodrigues [b], Leandro R.S. Barbosa [b], Walid A. Houry [c,d], Carlos H.I. Ramos [a,*]

[a] Institute of Chemistry, University of Campinas UNICAMP, Campinas, SP 13083-970, Brazil
[b] Institute of Physics, University of São Paulo, São Paulo, SP 05508-090, Brazil
[c] Department of Biochemistry, University of Toronto, Toronto, Ontario M5S 1A8, Canada
[d] Department of Chemistry, University of Toronto, Toronto, Ontario M5S 3H6, Canada

ARTICLE INFO

Article history:
Received 19 February 2020
Received in revised form 29 March 2020
Accepted 5 April 2020
Available online 14 April 2020

Keywords:
Hsp90
Aedes
Protein folding
Protein structure and function

ABSTRACT

Cellular proteostasis is maintained by a system consisting of molecular chaperones, heat shock proteins (Hsps) and proteins involved with degradation. Among the proteins that play important roles in the function of this system is Hsp90, which acts as a node of this network, interacting with at least 10% of the proteome. Hsp90 is ATP-dependent, participates in critical cell events and protein maturation and interacts with large numbers of co-chaperones. The study of Hsp90 orthologs is justified by their differences in ATPase activity levels and conformational changes caused by Hsp90 interaction with nucleotides. This study reports the characterization of Hsp90 from *Aedes aegypti*, a vector of several diseases in many regions of the planet. *Aedes aegypti* Hsp90, AaHsp90, was cloned, purified and characterized for its ATPase and chaperone activities and structural conformation. These parameters indicate that it has the characteristics of eukaryotic Hsp90s and resembles orthologs from yeast rather than from human. Finally, constitutive and increased stress expression in *Aedes* cells was confirmed. Taken together, the results presented here help to understand the relationship between structure and function in the Hsp90 family and have strong potential to form the basis for studies on the network of chaperone and Hsps in *Aedes*.

© 2020 Elsevier B.V. All rights reserved.

1. Introduction

Hsp90 is a molecular chaperone involved in the important protein quality control (PQC) system, acting in client-protein folding and regulation, and in the assembly of protein complexes [1–4]. Additionally, Hsp90 is essential for eukaryotic cell growth; it is a hub protein, since it interacts with over 10% of the proteome [5] and thus is a very abundant protein, representing 1 to 3% of cytoplasmatic soluble proteins, in physiological conditions in mammalian cells [6].

Hsp90 is a dimeric protein, with each protomer being composed of three domains that have characteristic features. The nucleotide-binding N-terminal domain, the client-protein interaction Middle (M) domain, and the dimerization C-terminal domain. N and M domains are connected by a flexible charged linker, which is very important for protein dynamics and ATPase activity [7]. Two residues that participates in ATP hydrolysis, R380 and Q384 (yeast Hsp82 numbering) are located at the M domain [8]. The C-terminal contains the MEEVD motif responsible for the interaction with TPR co-chaperones [9]. Finally, all hydrophobic exposed surfaces, which are important for client-protein interaction, are present in all three domains of Hsp90s [10].

The ATPase activity of Hsp90 is essential for the protein *in vivo* activity [11,12]. Moreover, its ATPase cycle involves conformational changes whereby locally the N-terminal lid closes upon ATP binding, and globally the N-terminal domain transiently dimerizes [13,14]. Due to these conformational changes, Hsp90s have low ATPase activity, which is modulated by co-chaperones [15] that are also involved in the chaperone's specificity to client proteins [16]. However, these conformational changes are not the same in all species, since the global changes are not observed for all Hsp90s [17]. Thus, the study of Hsp90 orthologs is justified to increase the general knowledge regarding this protein. With that in mind, in this work, we aimed to characterize the Hsp90 from *Aedes aegypti*, since this mosquito is very important in tropical countries as it transmits many arboviruses including Dengue, Zika and Chikungunya [18]. The characterization of this protein is crucial for the understanding of the proteostasis maintenance mechanisms in

Abbreviations: CD, circular dichroism; Hsp, heat shock protein; SAXS, small-angle X-ray scattering; SEC-MALS, size exclusion chromatography coupled to multi-angle light scattering.

* Corresponding author.
E-mail address: cramos@iqm.unicamp.br (C.H.I. Ramos).

https://doi.org/10.1016/j.ijbiomac.2020.04.029
0141-8130/© 2020 Elsevier B.V. All rights reserved.

this organism, and hopefully can be translated into intervention strategies against the mosquito.

2. Material and methods

2.1. Sequence identification and analysis

The amino acid sequence for AaHsp90 was found with the NCBI BLASTp tool (https://blast.ncbi.nlm.nih.gov/Blast.cgi), using the human Hsp90α amino acid sequence as a template, against the *Aedes aegypti* protein databank. The global alignment of the full-length AaHsp90 (NCBI RefSeq: XP_001649752.1) amino acid sequence with its orthologs was performed using Clustal Omega software (https://www.ebi.ac.uk/Tools/msa/clustalo/). The sequences used were as follows: DmHsp90 (*Drosophila melanogaster* Hsp90, NCBI RefSeq: NP_523899.1), LbHsp90 (*Leishmania braziliensis* Hsp90, NCBI RefSeq: XP_001567804.1), yHsp82 (*Saccharomyces cerevisiae* Hsp90, NCBI RefSeq: NP_015084.1), hHsp90α (human Hsp90 α isoform, NCBI RefSeq: NP_005339.3), hHsp90β (human Hsp90 β isoform, NCBI RefSeq: NP_031381.2) and SsHsp90 (*Saccharum* sp. Hsp90, NCBI RefSeq: AGC60019.1). The identity and similarity between the sequences were determined using the NCBI BLAST Global Alignment tool (https://blast.ncbi.nlm.nih.gov/Blast.cgi).

2.2. Cloning, expression and purification

The AaHsp90 DNA coding sequence was optimized for expression in *Escherichia coli* and cloned into a pET28a vector between *Nde*I and *Xho*I restriction sites, introducing a TEV cleavage site and adding a His tag. Protein expression was carried out using *E. coli* strain BL21 (DE3) transformed with the constructed plasmid. Cells were grown in LB media with 30 μg mL^{-1} kanamycin, at 37 °C until an OD_{600} of about 0.8 was reached. Expression was induced by adding 0.5 mM IPTG, at 18 °C. After 18 h cells were harvested by centrifugation at 2450*g* for 15 min at 4 °C. Pellet was resuspended in 25 mM Tris-HCl, 200 mM NaCl, pH 8.0 (buffer A) and incubated with 1 mM PMSF, 30 μg mL^{-1} lysozyme and 5 U of DNAse for 30 min on ice. Cells were lysed using sonication and then centrifuged at 20,000*g* for 30 min at 4 °C.

Chromatographic purification was conducted first on a nickel affinity column (HisTrap™ HP, GE Healthcare Lifesciences) equilibrated with buffer A, and elution was carried out using a linear gradient of 0 to 500 mM imidazole. Eluted AaHsp90 was dialyzed against buffer A, and then incubated with CIP (Calf Intestinal Alkaline Phosphatase, New England Biolabs) overnight at 4 °C for nucleotide hydrolysis. Then, size exclusion chromatography was conducted using a Superdex 200 XK 26/60 column (GE Healthcare Lifesciences) equilibrated with buffer A. Eluted fractions were incubated with TEV protease overnight at 4 °C and then submitted to an affinity chromatography for TEV removal. Proteins were analyzed using SDS-PAGE and His-tag cleavage was confirmed by western blot analysis using a monoclonal anti-His antibody (GE Healthcare Lifesciences). Protein concentration was determined spectrophotometrically using the Edelhoch method [19]. Purity percentage was calculated using ImageJ software [20].

2.3. Secondary structure determination

Circular dichroism (CD) measurements were conducted using a Jasco J-810 spectropolarimeter with a Peltier-type temperature controller (Jasco Inc., Easton, MD, USA). CD spectra were acquired from 260 to 201 nm, using 2 μM AaHsp90 in a 2 mm quartz path length cuvette at 20 °C. Spectra were normalized to the mean residual molar ellipticity ([θ]) and the α-helix content was calculated as previously described [21].

2.4. Hydrodynamic parameters characterization

For analytical size exclusion chromatography (aSEC) experiments, AaHsp90 (apo, ATPγS-, ADP- and AMP-bound) was loaded onto a Superdex 200 GL 10/300 column (GE Lifesciences) equilibrated with 25 mM Tris-HCl, 200 mM NaCl pH 8.0, with elution monitored at 280 nm in an AKTA FPLC system (GE Lifesciences). The concentration of AaHsp90 was 15 μM and the nucleotides were 1.5 mM. Standard proteins with known Stokes radius (R_s) were used for calibration, at a concentration of approximately 2 mg mL^{-1}. Blue dextran at 0.8 mg mL^{-1} was used for column void determination. Protein retention volumes were transformed into partition coefficients (Kav) and a calibration curve was constructed using the R_s of the standard proteins as a function of $-(\log Kav)^{1/2}$. Linear fitting analysis was used to obtain the R_s of AaHsp90.

Size exclusion chromatography and multi-angle light scattering (SEC-MALS) experiments were conducted using an AKTA FPLC instrument (GE Healthcare Lifesciences) coupled to a miniDAWN TREOS light scattering detector and to an Optilab T-rEX refractive index detector (Wyatt Technology). Experiments were carried out at room temperature, using a Superdex 200 GL 10/300 column (GE Healthcare Lifesciences) and the protein concentration was 10 μM. Data analysis was conducted with the Astra 6 software (Wyatt Technology).

Dynamic light scattering (DLS) measurements were performed in a Malvern Zetasizer Nano ZS 90 (Model 3690) instrument equipped with a 633 nm laser, in a polystyrene cell, at 20 °C. AaHsp90 was used at concentrations of 10, 50 and 100 μM. Nucleotide-bound forms (ATPγS, ADP and AMP-bound) were at 10 μM and the nucleotides at 1 mM.

2.5. Small angle X-ray scattering (SAXS)

Small angle X-ray scattering (SAXS) data were acquired at the D11A-SAXS1 beamline in the Brazilian National Laboratory of Synchrotron Light (LNLS – CNPEM, Campinas, Brazil, proposal 20190061). Measurements were performed using AaHsp90 (apo, ATPγS-, ADP- and AMP-bound) at 2.5 mg mL^{-1} (30 μM) with nucleotides at 3 mM, in buffer 25 mM Tris-HCl, 200 mM NaCl, pH 8.0 at 25 °C, inside a 1 mm mica cell positioned at a ~1000 mm distance from the detector (scattering vector range of $0.15 < q < 3.3\ nm^{-1}$) and exposed to a monochromatic X-ray beam ($\lambda = 1.488$ Å). Frames of 100 s were measured and averaged to increase the signal-to-noise ratio, improving the scattering curve quality.

SAXS curves were corrected by incident X-ray intensity, sample's attenuation and buffer contribution. Guinier analysis [22,23] was performed using PRIMUS software [24,25], and calculating both radius of gyration, Rg, and the forward intensity at zero angle, I(0), which are related to the protein molecular mass [26]. Moreover, a Fourier Transform connects the pair distance distribution function, p(r), to the scattering intensity, I(q). The p(r) function is related to the protein form factor, in the absence of interference functions. These functions were calculated using GNOM software [27]. Primary assessment for low resolution protein envelope reconstruction was performed with the AMBIMETER software, which is able to evaluate protein envelope ambiguity on 3D reconstructions [28]. *Ab initio* analysis was performed by simulated annealing using beads as dummy atoms with the program DAMMIF [29], generating twenty different structures with P2 symmetry which were then averaged using DAMAVER [30,31], generating a final averaged model. Finally, DAMMIN [32] was used to refine the protein envelope. Additional modelling was performed using a hybrid rigid body method and the PDB entries 1BYQ [11] and 3HJC (DOI: https://doi.org/10.2210/pdb3HJC/pdb) as templates for the N-terminal domain and M and C-terminal domains, respectively. SwissModel was employed to use these templates to model the two regions according to the AaHsp90 sequence. These modelled structures were used as rigid bodies in the program BUNCH [33] to search for relative domain orientations, with non-

resolved residues modelled *ab initio* as beads. Noteworthy, BUNCH selects the structure that minimizes the discrepancy (χ^2) with the experimental data by rearranging the PDB structures' orientation within the distance constraint and modelling linkers as beads. P2 symmetry was applied (AaHsp90 dimers) and constraints were applied using previously published contact information as reference [34]. Fits were evaluated by the χ^2 and p-value quantities [35].

2.6. Chaperone activity

Porcine mitochondrial citrate synthase (CS), 1 μM, was preincubated with AaHsp90 for 5 min in a 1:1 proportion (monomeric concentration) in the absence and in the presence of 100 μM nucleotides (ATPγS, ADP and AMP). After preincubation, light scattering (turbidity) was monitored at 320 nm for 2000 s in an Aminco Bowman Series 2 (SLM-Aminco) fluorometer with controlled temperature at 42 °C. Controls were: CS alone, AaHsp90 alone and CS in the presence of Bovine serum albumin (control for a protein without chaperone activity). Results are the average of at least three independent experiments.

2.7. ATPase activity measurement

For measurements of ATPase activity, the ATP/NADH coupled method was conducted [36]. Briefly, reactions were comprised of 3 mM PEP (phosphoenolpyruvate), 0.3 mM NADH, 40 U mL^{-1} PK, 58 U mL^{-1} LDH in a buffer containing 25 mM Tris-HCl, 200 mM NaCl, 8 mM $MgCl_2$, pH 8.0. ATPase activity was assayed by addition of ATP (pH 7.0) in the concentrations of 1, 2, 3, 4 and 5 mM. Rate of NADH oxidation, which is proportional to ATPase activity, was monitored through loss of absorbance at 340 nm. Readings were taken at 37 °C every 1 min for 1.5 h in a plate reader (BioTek Instruments Inc.). AaHsp90 concentration in the reaction was 10 μM (monomer).

2.8. In cell experiments

Aedes albopictus C6/36 cells were cultivated in 6-well plates with Eagle's Minimum Essential Medium supplemented with 10% fetal bovine serum, at 28 °C and 5% CO_2, until confluence. For the heat treatment, cells were incubated at 37 °C for 90 min [37], washed with ice-cold PBS and detached from the plate using trypsin. For trypsin removal, cells were washed three times with ice-cold PBS by centrifugation at 1200*g* for 5 min at 4 °C. Then, cells were lysed in RSB-NP40 buffer (1.5 mM $MgCl_2$, 10 mM Tris–HCl, 10 mM NaCl and 1% Igepal CA 630) in the presence of protease inhibitor cocktail (500 μM AEBSF/mL, 150 nM aprotinin/mL, 1 μM E-64 protease inhibitor/mL, 0.5 mM EDTA/mL, 1 μM leupeptin/mL, Calbiochem). After incubation for 2 min on ice, cells were centrifuged at 12,000*g* for 15 min at 4 °C. Soluble proteins were mixed with sample buffer, boiled for 5 min and then loaded onto SDS-PAGE. Western blot analysis was conducted using a nitrocellulose 0.45 μm membrane and transferring was carried out in a semi-dry apparatus. Human Hsp90α (1:2000) (StressMarq Biosciences Inc., SMC-147) and β-actin (1:5000) (Abcam, ab184220) monoclonal antibodies were primary and goat-produced polyclonal anti-mouse IgG (1:5000) conjugated to HRP (Abcam, ab6789) was secondary. Membranes were developed using the ECL kit (Ge Healthcare) and observed using the Imager 600 instrument (Ge Healthcare). Bands were quantified using ImageJ software. Statistical analysis was conducted in the GraphPad Prism 5 software and the Student's *t*-test was applied to the data.

3. Results and discussion

3.1. The Hsp90 from Aedes aegypti

Hsp90 is one of the major chaperones in the cell, it is ubiquitous and is a hub protein that interacts with about 10% of the proteome in yeast [38–40]. Characteristically, Hsp90s contain three domains: N (at the N-terminus), M (Middle, locate in the central part) and C (at the C-terminus and containing the MEEVD motif). All these domains were identified in AaHsp90 by alignment (Fig. 1A and B). AaHsp90 shares 63 to 85% identity and 78 to 92% similarity with the sequence of its orthologs (Table 1). The alignment shows that the residues reported to be important for ATP binding [14,41] are conserved in AaHsp90 (Fig. 1B). Likewise, the residues that compose the lid region [14] are also conserved and are formed by residues 99 to 130 in AaHsp90, as shown in Fig. 1B (in bold). Additionally, the residues involved in the catalytic center for ATP hydrolysis [14], Q385 (yeast Hsp82 numbering) [8] and the exposed hydrophobic regions important for client-protein interaction [10] are also conserved (Fig. 1B). Finally, AaHsp90 has the conserved MEEVD motif, which is important for interaction with TPR co-chaperones [42], in the C-terminal domain (Fig. 1B).

3.2. AaHsp90 is a folded elongated homodimer in solution and nucleotides have no significant effect on its global conformation

AaHsp90 was produced with high purity (>95%) (Fig. S1) and appears as a band of about 82 kDa on SDS-PAGE gel (Fig. 2A). The His-tag was efficiently cleaved by TEV protease, as shown by western blot analysis (Fig. 2B). The secondary structure was evaluated by CD showing the presence of two minima at 208 and 222 nm in the spectrum, characteristic of an α-helical protein (Fig. 2C). The percentage of α-helix was calculated as of about 35%, which is in good agreement with results of Hsp90s from other organisms [43–50].

The hydrodynamic parameters of AaHsp90 were then investigated. SEC-MALS showed that AaHsp90 eluted as a single peak with molecular mass of 160.1 ± 2.2 kDa (Fig. 3A), a value compatible with that of a dimer (predicted value equals to 163 kDa). As a matter of fact, the dimerization of Hsp90s by their C-termini is well established [34]. Stokes radius (R_s) (Fig. 3B) and diffusion coefficient (D) were calculated as 65.6 ± 0.2 Å and 2.7 ± 0.3 × 10^{-7} cm^2 s^{-1}, respectively. These values are in agreement with those reported for Hsp90 orthologous [43,47,48]. The obtained R_s and D values suggest that AaHsp90 is an elongated protein, because these values differ substantially from those predicted for a non-hydrated sphere with the same molecular mass (Table 2) [51]. This is in agreement with what is known for other Hsp90 proteins [45,46,50] and with the SAXS investigation of AaHsp90 (see below). However, it is important to mention that the addition of either ATPγS, ADP or AMP had no effect on R_s or D (Table 2; see also discussion below).

The effect of nucleotides on the conformation of AaHsp90 was also evaluated by small angle X-ray scattering (SAXS). SAXS was used to measure the radius of gyration (R_g), maximum dimension (D_{max}) and also to obtain low-resolution structural conformations of AaHsp90-apo, AaHsp90-ATPγS, AaHsp90-ADP and AaHsp90-AMP in solution. However, the presence of the nucleotides did not result in any significant change in the general SAXS profile (Figs. S2 and S3 and Table S1).

Fig. 4A shows the SAXS curves and the Guinier analysis (inset) for the apo form of AaHsp90. R_g and I(0) values were validated by Guinier Peak Analysis (Fig. S2), which is a tool to assess protein flexibility and to validate the chosen Guinier region [58]. As showed by other experiments (see above), the addition of either ATPγS, ADP or AMP had no significant effect on SAXS curves. Thus, since the SAXS curves of all studied systems are quite similar, only the SAXS analysis of the AaHsp90-apo form is further discussed (however, see tables and figures for information on the evaluation of nucleotide addition). Guinier plot showed a linear behavior in the small-q range indicating that the protein was a monodisperse system at these conditions and allowed for the calculation of the radius of gyration (Rg), which was 6.36 ± 0.11 nm for AaHsp90-apo (see also Table S1 and note that this value was indistinguishable from those in the presence of nucleotides), being slightly longer when compared to the R_g reported for either *Leishmania braziliensis* Hsp90 (5.56 ± 0.30 nm [59]) or porcine Hsp90 (5.46 ± 0.20 nm [60]). In addition, Kratky analysis indicates that AaHsp90-apo is folded and

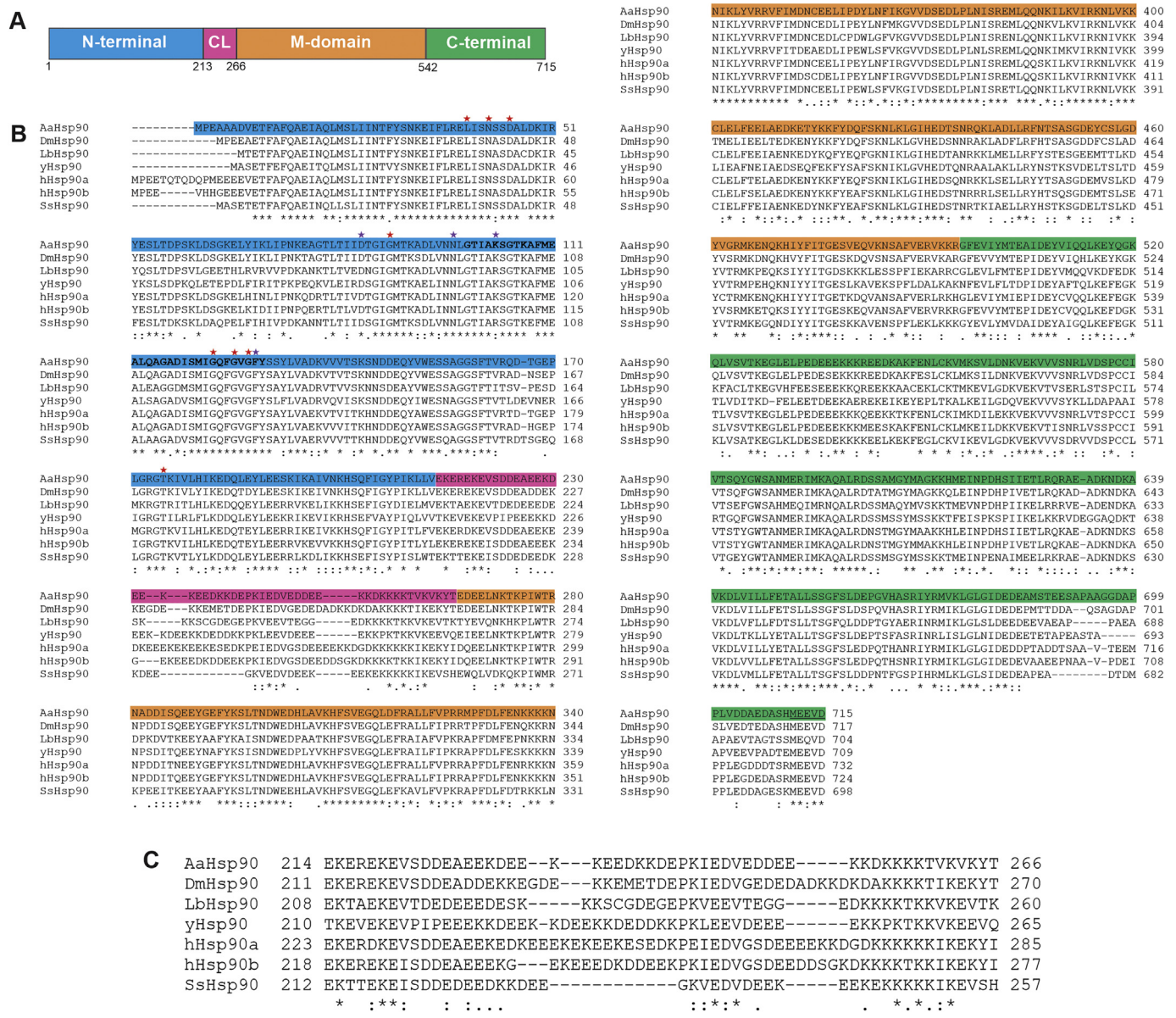

Fig. 1. AaHsp90. A) Schematic representation of AaHsp90 domains (N, M and C) organization. CL: charged linker. B) Sequence alignment of AaHsp90, DmHsp90 (*Drosophila melanogaster*), LbHsp90 (*Leishmania braziliensis*), yHsp90 (yeast, *Saccharomyces cerevisiae*), hHsp90a (human, *Homo sapiens*), hHsp90b (human, *Homo sapiens*) and SsHsp90 (sugarcane, *Saccharum* sp.). Blue: N-terminal domain, CL: charged linker region, orange: Middle domain, green: C-terminal domain. red stars: residues involved in directly binding to adenosine nucleotides. Purple stars: residues involved in binding to adenosine nucleotides through a water molecule. Bold residues: lid region. Underlined residues: MEEVD motif. C) Partial sequence alignment (as in B) highlighting the charged linker region.

composed mainly of globular domains with the presence of flexible regions, most likely interdomain linkers, as indicated by the bell-shaped profile of the curves, but still deviating from an ideal globular profile (Guinier law, represented as dashed lines) (Fig. 4B, inset). This result agrees nicely with the conformation of Hsp90s, since all three domains are well-folded.

Table 1
Percentage of sequence identity and similarity of AaHsp90 with its orthologs.

Protein	Organism	Identity (%)	Similarity (%)
DmHsp90	*Drosophila melanogaster*	85	92
hHsp90α	*Homo sapiens*	79	88
hHps90β	*Homo sapiens*	79	88
SsHsp90	*Saccharum* sp.	69	83
LbHsp90	*Leishmania braziliensis*	64	79
yHsp82	*Saccharomyces cerevisiae*	63	78

The molecular mass of AaHsp90-apo can also be estimated by SAXS using two different approaches. The first uses water as standard scattering curve [61] and gives a molecular mass of 130.4 kDa. The second uses the concentration independent method, recently developed [62], which also uses ATSAS package and is further processed by Bayesian assessment, to determine the molecular mass of 169.6 kDa. Such values are in reasonable agreement with each other since SAXS is not a highly precise tool for molecular mass determination. Nevertheless, both of these values indicate that AaHsp90 is dimeric, a result in agreement with the SEC-MALS data.

Moreover, according to the pair-distance distribution function, p (r) (Fig. 4B), AaHsp90-apo has a non-spherical, quite elongated shape with a D_{max} of 21.0 ± 1.0 nm and maximum of frequencies (peak position) at approximately 3.5 nm. It is worth mentioning that these values are longer than those reported for yeast Hsp82, *Homo sapiens* Hsp90α and *Leishmania braziliensis* Hsp90 [59,63]. The calculated structural parameters for all samples are present in Table S1, showing very similar

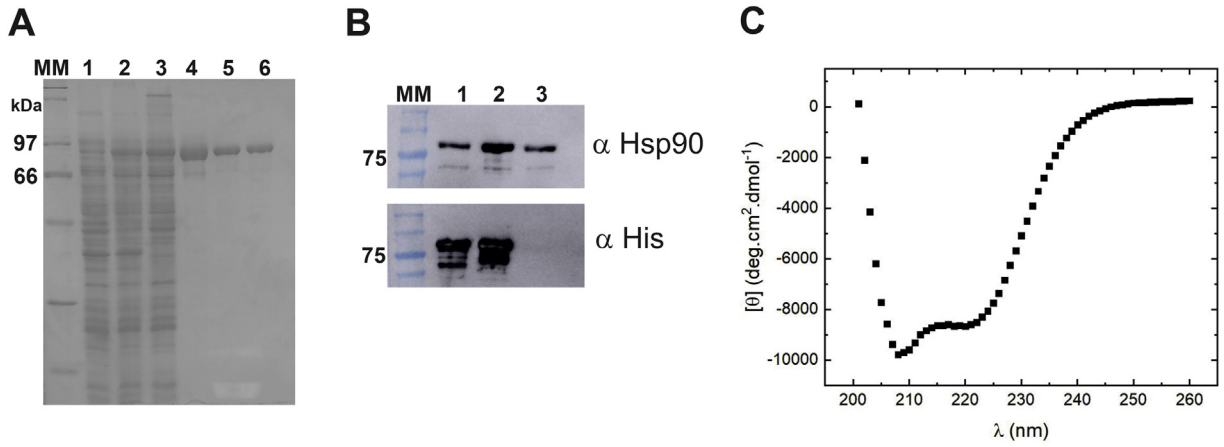

Fig. 2. AaHsp90 was produced with high purity and folded. A) SDS-PAGE. MM: molecular marker. 1: Non-induced, 2: total fraction obtained after *E. coli* lysis, 3: soluble fraction of lysis, obtained after centrifugation, 4: fraction obtained from affinity chromatography, 5: fraction obtained from gel filtration chromatography, 6: his-tag cleaved AaHsp90, after the second affinity chromatography. For details see Fig. S2. B) Western-blot analysis, confirming his-tag cleavage. 1: fraction obtained from affinity chromatography, 2: fraction obtained from size exclusion chromatography, 3: his-tag cleaved AaHsp90, after the second affinity chromatography. C) Circular dichroism spectrum of AaHsp90, showing a well-folded and mainly α-helical protein. The α-helix content was of about 35%.

values. Guinier Peak Analysis, p(r) functions and dimensionless Kratky plots for all samples are also presented in the supplemental material (Fig. S3) and also yield similar results. Thus, combined with the hydrodynamic analyses, it seems that nucleotide binding does not alter the protein conformation in a magnitude detectable by low resolution methods, like SAXS.

To further investigate AaHsp90 conformation, the AMBIMETER software was used and generated a value of 2.68 for the low resolution structure, indicating an elevated degree of ambiguity score suggesting that it is necessary to use a constrain to calculate a reliable protein envelope [28]. Thus, according to several SAXS data reported in the literature for different Hsp90 orthologs, a P2 symmetry was imposed for the calculation of the AaHsp90 envelope. Fig. 4D displays the final *ab initio* envelope, revealing an open conformation in agreement with reported data for the apo forms of yeast Hsp82, human Hsp90α, LbHsp90, porcine Hsp90 and HtpG [59,60,63]. As a further demonstration of the reliability of the model, the structure obtained by hybrid rigid body modelling (using BUNCH) (Fig. 4D) fits the experimental scattering curve (Fig. 4C) for AaHsp90-apo and follows the same general structural features as the envelope. It is known that Hsp90s shows different amplitudes of aperture [50,60] as well as an equilibrium between opened and closed conformations in the apo state [17,59]. However, nucleotides had no significant effect on the protein conformation, indicating that all studied systems have an open conformation, since the SAXS curves are alike (Fig. S2).

The results in the presence of nucleotides may come as a surprise since the ATPase cycle of Hsp90s usually involves global conformational changes of Hsp90 [13,14,64]. However, the magnitude of the conformational changes differs between species and, in some cases, global changes are not observed at all [17,65], as for instance for canine GRP94 [45] and human Hsp90. As a matter of fact, only a small fraction of human Hsp90s presented global conformational changes in response to nucleotide binding, as previously reported by negative-stain electron microscopy [17]. Graf and co-workers [66] used a hydrogen exchange approach to evaluate the conformational cycles of Hsp90s from a variety of organisms and concluded that eukaryotic Hsp90s are much more flexible than its *E. coli* counterpart and that nucleotides induce only minor changes in conformation. They showed that eukaryotic Hsp90s are as dynamic in the absence of nucleotides as in the presence of it, indicating that those proteins have many conformational states separated

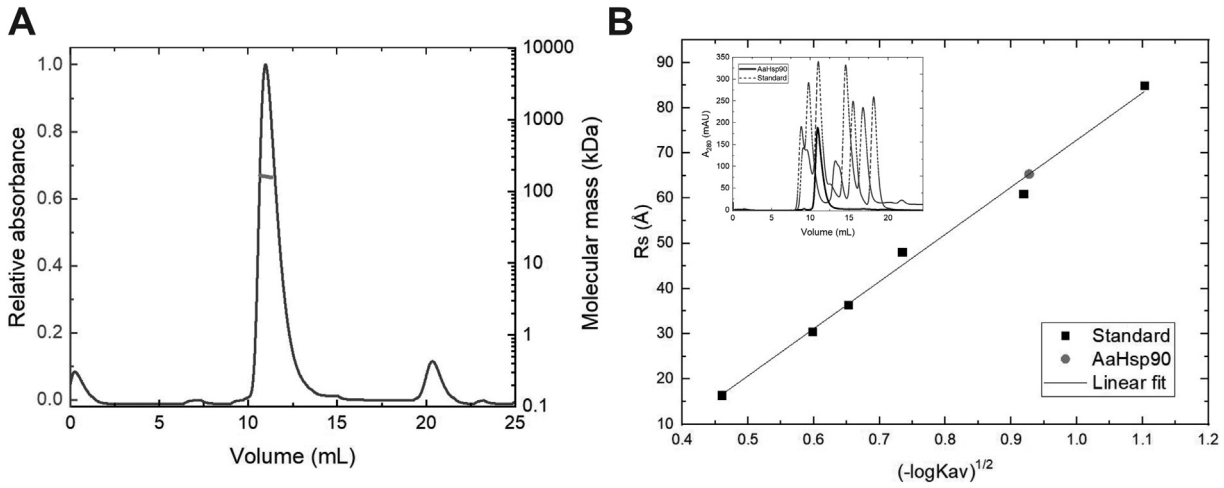

Fig. 3. Hydrodynamic characterization of AaHsp90. A) SEC-MALS. Molecular mass in solution was 160.1 ± 2.2 kDa, corresponding to a dimer. B) Analytical size exclusion chromatography (aSEC). Stokes radius (R_s) was 65.6 ± 0.2 Å. Inset: chromatogram of AaHsp90 and standard proteins, which elution volumes were converted to $(-\log Kav)^{1/2}$ and used to construct the calibration curve showed in B.

Table 2
Measured *versus* predicted[a] hydrodynamic parameters.

Parameter	AaHsp90	Predicted[a]
R_s (Å)	65.6 ± 0.2[b]	36.1[c]
D ($cm^2\ s^{-1}$)	$2.7 \pm 0.3 \times 10^{-7}$	6.8×10^{-7}

[a] For a non-hydrated sphere with the same molecular mass of AaHsp90 dimer (see Borges and Ramos [51] for equations).
[b] For the apo form, for AMP and ATPγS forms are 65.8 and for ADP is 65.9.
[c] For all forms.

by small energy barriers. This conclusion is supported by the findings of this work. Additionally, it is worth noting that a closed conformation is obtained when Hsp90 is stabilized by co-chaperones, as p23 [44].

Also interesting is the fact that analyses of the disordered region between the N- and middle- domains, also known as charged linker (CL), support the results of this work. The sequence identity among Hsp90s when considering just the CL is lower among species (see Fig. 1C). Hainzl and co-workers [7] showed that increased deletions of the CL from yeast Hsp90 decreased the dimerization of the N-terminal domain. Tsutsumi and co-workers [67] changed the residue composition and length of this domain and found variation in both function and conformation. The authors showed that replacement of the CL from human Hsp90α with that from yeast Hsp90 increased trypsin sensitivity. Jahn et al. [68] showed that CL needs to be in contact with the N-domain to be structured and modulates the dimerization of this domain.

We found that the CL region of AaHsp90 is more similar to yeast Hsp90 (yHsp90) than to human (hHsp90). The negative net charge of the linker is −8 for yeast (residues 210–265) and −12 for human Hsp90α (residues 223–285), while it has an intermediate value of −10 in *Drosophila* (residues 211–270). In *Aedes* (residues 214–266), it is similar to yeast, −8. Additionally, Tsutsumi and co-workers [69] showed that a beta-sheet region adjacent to CL is important for the conformation, as mutants in the hydrophobic positions IxL in both yeast (residues 205–207) and human (residues 218–220) Hsp90s abolished the N-terminal dimerization in the presence of ATP. They showed that the interaction of this region with the CL is responsible for function. It is interesting to notice that, although I and L are conserved, the x position is Q in yeast and T in human, but K in *Aedes*. Q and K have almost the same size and side-chain conformational entropy, being usually replaced by each other to improve protein crystallization [70].

3.3. Functional evaluation

A core experiment for molecular chaperones is the evaluation of their capacity to protect model proteins against aggregation caused by thermal- or chemical-induced unfolding. Citrate synthase is a model protein used in such experiments because it aggregates as a function of temperature and this phenomenon can be followed by the turbidity of the sample as measured by light scattering. See, for instance results using Hsp90s from *Citrus sinensis*, *Saccharum* spp. and *Leishmania braziliensis* [1–3]. Fig. 5 (raw data is shown in Fig. S4) shows that AaHsp90 was able to protect CS against aggregation: reduction of about 75%. Furthermore, the addition of nucleotides had no significant effect on this activity (Figs. 5 and S4). This experiment shows that AaHsp90 has chaperone activity.

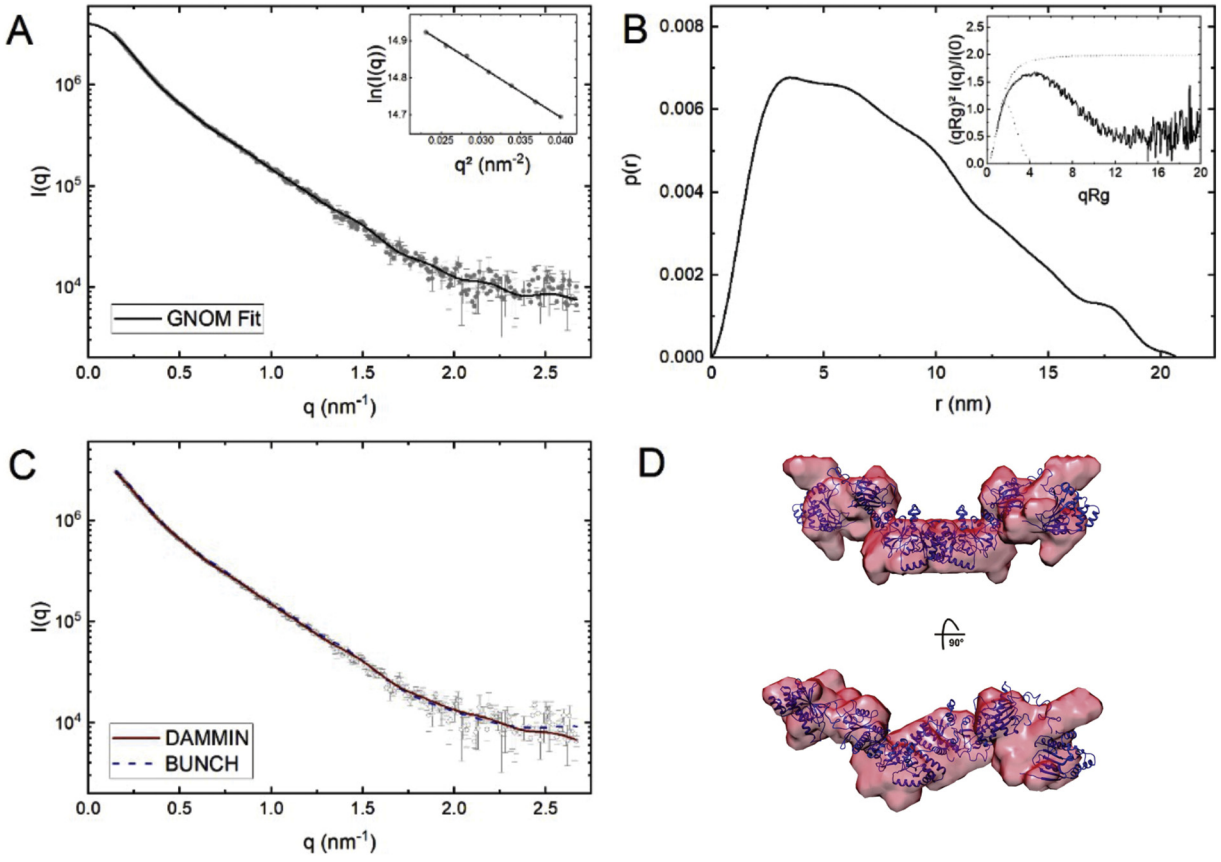

Fig. 4. SAXS analysis of AaHsp90. A) Collected data for the apo form (filled circles) and GNOM fitting used for calculation of the p(r) function. Guinier plot (inset) linearization resulted in a R_g of 6.36 ± 0.11 nm. B) p(r) function, showing a very elongated profile in solution with D_{max} of 21.0 ± 0.1 nm. The dimensionless Kratky plot (inset) shows that the protein has well folded domains with some degree of flexibility explained by the profile (solid line) being intermediate between a rigid globular protein (dashed line) and a random Gaussian chain (short dotted line) with a pronounced bell-shape. C) DAMMIN (red solid line) and BUNCH (blue dashed line) software fittings to the experimental data (empty circles). D) Aligned 3D models for AaHsp90, generated by *ab initio* (red surface) and hybrid rigid-body (blue cartoon) modelling. See text for details.

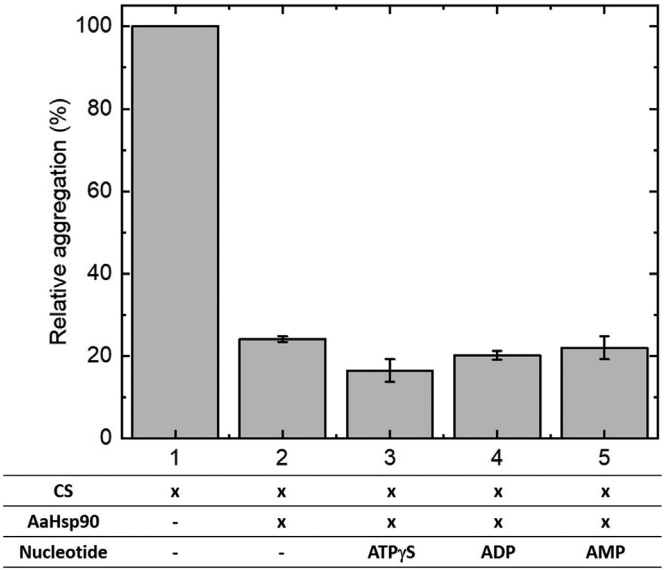

Fig. 5. Chaperone activity. Citrate synthase (CS) aggregates as a function of temperature and the aggregation can be followed by the turbidity measured by light scattering (see raw data on Fig. S4). CS aggregation was set as 100% (bar 1) and AaHsp90 was able to protect CS against aggregation by reducting it to about 25% (bar 2). The presence of nucleotides (ATPγS: bar 3, ADP: bar 4, or AMP: bar 5) had no significant effect on AaHsp90 activity.

Although the nucleotides tested had no effect neither on the hydrodynamic parameters nor on chaperone activity of AaHsp90, this protein was able to hydrolyze ATP. AaHsp90's ATPase activity was evaluated and the kinetic parameters fitted using Michaelis-Menten equation (Fig. 6). The values of K_M and k_{cat} were 2.32 ± 0.46 mM and 1.28 ± 0.10 min^{-1}, respectively, which gives a catalytic efficiency (k_{cat}/K_m) of 5.51×10^{-4} min^{-1} μM^{-1}. Although K_m and k_{cat} are somehow higher than those reported for other orthologous, the catalytic efficiency is in the same range as those previously reported [11,12,43,45,52–57]. For instance, Richter et al. [55] showed that human and yeast Hsp90 proteins undergo similar ATP-dependent conformational changes, despite having different ATPase rates. Altogether, these results demonstrate that AaHsp90 binds nucleotides and is functional.

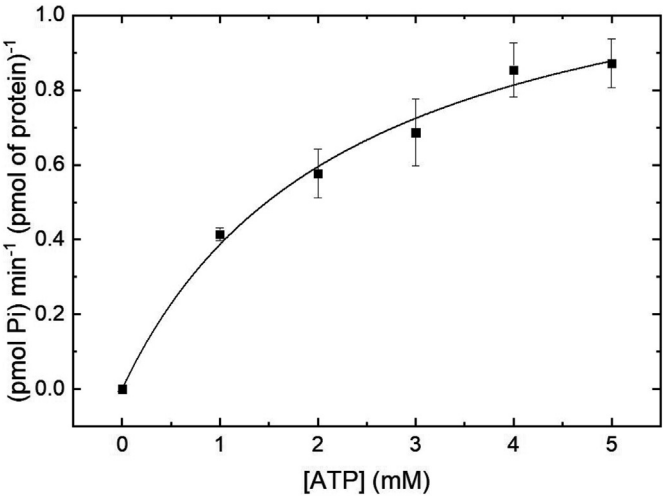

Fig. 6. ATPase activity. A_{340nm} values (from NADH oxidation) were converted to pmol of Pi per pmol of protein. The obtained values (black squares) were then fitted by Michaelis-Menten analysis (curve), which gave the kinetics parameters of $K_M = 2.32 \pm 0.46$ mM and $k_{cat} = 1.28 \pm 0.10$ min−1, which means a catalytic efficiency (k_{cat}/K_M) of 5.51×10^{-4} min^{-1} μM^{-1}. Mean and standard deviation of three independent experiments.

3.4. Hsp90 had increased expression upon heat-shock treatment in Aedes cells

After investigating the structure and function of the Hsp90 from *Aedes*, we asked whether this protein is expressed in *Aedes* cells and if that expression increases upon stress. As a matter of fact, AaHsp90 was identified in *Aedes albopictus* cells and its expression was upregulated upon heat shock stress (Fig. 7A). Fig. 7B shows the mean and standard deviation of 5 experiments. Statistical analysis was applied to the data and it was significant ($p < 0.005$).

It is, to our knowledge, the first time that the heat shock-induction of AaHsp90 expression is shown at protein level, although it has been shown by mRNA after heat shock in larvae, pupae and adult mosquitos [71–73]. In fact, it was previously shown an increase in the expression of a 83-kDa protein in *Aedes albopictus* cells upon heat shock treatment, however this protein was not identified in the study [37,74] try to reword.

4. Conclusion

Hsp90 interacts with approximately 10% of the cellular proteome and plays an important role in signaling. The strategy of studying Hsps from different organisms is crucial to better understand the characteristics of these proteins and their interaction with components of the chaperone, an approach that has proven to be successful because important differences have been identified between orthologs. Such studies have helped to advance the general knowledge about the relationship between structure and function in Hsp90.

In this study, we present the first cloning and characterization of Hsp90 from *Aedes aegypti* (AaHsp90). This mosquito is a vector of several diseases of global impact because recent studies have shown that with global warming this vector has expanded to regions that were not previously infested by it. AaHsp90 was purified folded and with characteristic features such as homodimer formation and having ATPase activity. However, no significant alteration in the conformation of the protein was observed upon nucleotide interaction. Nonetheless, the dimeric and elongated conformation of the protein was confirmed and a conformational model was generated from the SAXS experiments. Additionally, AaHsp90 has characteristic chaperone activity. Finally, an increase in the cellular expression of the protein has been identified under heat stress conditions.

Authorship contribution

N.G.Q.: Data collection, analysis and interpretation. G.M.S.P., L.R.S.B., L.F.C.R.: SAXS. W.A.H., C.H.I.R.: Data analysis and interpretation. W.A.H., C.H.I.R.: designed the work. All authors: drafted and critically reviewed the article.

Declaration of competing interest

The authors declare no competing interests.

Acknowledgements

This work was supported by Global Affairs Canada (Canada) and CAPES (Brazil) to WAH and CHIR. This work was partially supported by FAPESP (2015/15822-1, 2012/01953-9, 2016/05019-0) and CNPq to LRSB who also holds a research fellowship from CNPq (306943/2015-8, 420567/2016-0). CHIR has a research fellowship from CNPq and FAPESP (2017/26131-5). This work was partially supported by a Canadian Institutes of Health Research Project grant (PJT-148564) to WAH. NGQ received fellowships from FAPESP (2014/25967-4) and CAPES (88887.137523/2017-00). LFCR received fellowship from CAPES (88882.332864/2019-01). Molecular graphics and analyses performed with UCSF Chimera, developed by the Resource for Biocomputing,

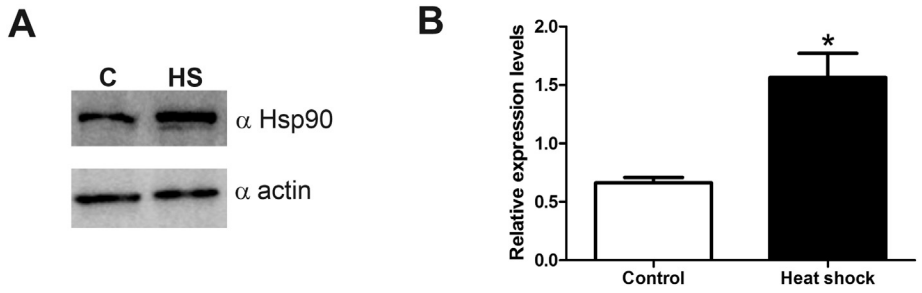

Fig. 7. Identification of AaHsp90 in *Aedes albopictus* C636 cells and evaluation of heat shock treatment on protein expression. A) Western blot analysis using anti-Hsp90 and anti-actin specific antibodies, showing that AaHsp90 was expressed in both control (C) and heat shock treatment (HS) cells. MM: molecular marker. B) Expression levels of AaHsp90 in both control and heat shocked cells, obtained from the quantification of western blot bands. AaHsp90 expression was upregulated upon heat shock stress.

Visualization, and Informatics at the University of California, San Francisco, with support from NIH P41-GM103311. The authors are also in debt with LNLS SAXS beamline staff for the use of their facilities. The authors also thank Dr. A. Z. B. Aragão for the technical support and Prof. Dr. J. L. P. Módena for gently providing C636 cells.

Appendix A. Supplementary data

Supplementary data to this article can be found online at https://doi.org/10.1016/j.ijbiomac.2020.04.029.

References

[1] J.C. Borges, C.H.I. Ramos, Protein folding assisted by chaperones, Protein Pept. Lett. 12 (2005) 257–261, https://doi.org/10.2174/0929866053587165.
[2] D.O. Pratt, B. William, Toft, regulation of signaling protein function and trafficking by the hsp90/hsp70-based chaperone machinery, Exp. Biol. Med. 228 (2003) 111–133.
[3] T. Makhnevych, W.A. Houry, The role of Hsp90 in protein complex assembly, BBA Mol. Cell Res. 1823 (2012) 674–682, https://doi.org/10.1016/j.bbamcr.2011.09.001.
[4] F.H. Schopf, M.M. Biebl, J. Buchner, The HSP90 chaperone machinery, Nat. Rev. Mol. Cell Biol. 18 (2017) 345–360, https://doi.org/10.1038/nrm.2017.20.
[5] R. Zhao, W.A. Houry, Molecular interaction network of the Hsp90 chaperone system, in: P. Csermely, L. Vígh (Eds.), Mol. Asp. Stress Response Chaperones, Membr. Networks. Adv. Exp. Med. Biol. Springer, New York, NY 2007, pp. 27–36, https://doi.org/10.1007/978-0-387-39975-1_3.
[6] B. Lai, W.N.W. Chin, A.E. Stanek, W. Keh, K.W. Lanks, Quantitation and intracellular localization of the 85K heat shock protein by using monoclonal and polyclonal antibodies, Mol. Cell. Biol. 4 (1984) 2802–2810.
[7] O. Hainzl, M.C. Lapina, J. Buchner, K. Richter, The charged linker region is an important regulator of Hsp90 function, J. Biol. Chem. 284 (2009) 22559–22567, https://doi.org/10.1074/jbc.M109.031658.
[8] P. Meyer, C. Prodromou, B. Hu, C. Vaughan, S.M. Roe, B. Panaretou, P.W. Piper, L.H. Pearl, Structural and functional analysis of the middle segment of Hsp90: implications for ATP hydrolysis and client protein and cochaperone interactions, Mol. Cell 11 (2003) 647–658.
[9] J. Buchner, Hsp90 & Co. – a holding for folding, Trends Biochem. Sci. 24 (1999) 136–141.
[10] K.A. Krukenberg, T.O. Street, L.A. Lavery, D.A. Agard, Conformational dynamics of the molecular chaperone Hsp90, Q. Rev. Biophys. 44 (2011) 229–255.
[11] W.M.J. Obermann, H. Sondermann, A.A. Russo, N.P. Pavletich, F.U. Hartl, In vivo function of Hsp90 is dependent on ATP binding and ATP hydrolysis, J. Cell Biol. 143 (1998) 901–910.
[12] B. Panaretou, C. Prodromou, S.M. Roe, R.O. Brien, J.E. Ladbury, P.W. Piper, L.H. Pearl, ATP binding and hydrolysis are essential to the function of the Hsp90 molecular chaperone in vivo, EMBO J. 17 (1998) 4829–4836.
[13] C. Prodromou, B. Panaretou, S. Chohan, G. Siligardi, R.O. Brien, J.E. Ladbury, S.M. Roe, P.W. Piper, L.H. Pearl, The ATPase cycle of Hsp90 drives a molecular 'clamp' via transient dimerization of the N-terminal domains, EMBO J. 19 (2000) 4383–4392.
[14] J. Li, L. Sun, C. Xu, F. Yu, H. Zhou, Y. Zhao, J. Zhang, J. Cai, C. Mao, Structure insights into mechanisms of ATP hydrolysis and the activation of human heat-shock protein 90, Acta Biochim. Biophys. Sin. Shanghai 44 (2012) 300–306, https://doi.org/10.1093/abbs/gms001.Advance.
[15] S. Sima, K. Richter, Regulation of the Hsp90 system, BBA Mol. Cell Res. 1865 (2018) 889–897, https://doi.org/10.1016/j.bbamcr.2018.03.008.
[16] J. Li, J. Soroka, J. Buchner, The Hsp90 chaperone machinery: conformational dynamics and regulation by co-chaperones, Biochim. Biophys. Acta Mol. Cell Res. 1823 (2012) 624–635, https://doi.org/10.1016/j.bbamcr.2011.09.003.
[17] D.R. Southworth, D.A. Agard, Species-dependent ensembles of conserved conformational states define the Hsp90 chaperone ATPase cycle, Mol. Cell 32 (2008) 631–640, https://doi.org/10.1016/j.molcel.2008.10.024.
[18] S.V. Mayer, R.B. Tesh, N. Vasilakis, The emergence of arthropod-borne viral diseases: a global prospective on dengue, chikungunya and zika fevers, Acta Trop. 166 (2017) 155–163, https://doi.org/10.1016/j.actatropica.2016.11.020.
[19] H. Edelhoch, Spectroscopic determination of tryptophan and tyrosine in proteins, Biochemistry. 6 (1967) 1948–1954, https://doi.org/10.1021/bi00859a010.
[20] C.A. Schneider, W.S. Rasband, K.W. Eliceiri, NIH Image to ImageJ: 25 years of image analysis, Nat. Methods 9 (2012) 671–675. http://www.ncbi.nlm.nih.gov/pubmed/22930834.
[21] D.H.A. Correa, C.H.I. Ramos, The use of circular dichroism spectroscopy to study protein folding, form and function, Afr. J. Biochem. Res. 3 (2009) 164–173. https://www.researchgate.net/profile/Daniel_Correa5/publication/228351774_The_use_of_circular_dichroism_spectroscopy_to_study_protein_folding_form_and_function/links/0c96051a39700a319c000000.pdf.
[22] A. Guinier, G. Fournet, Small Angle Scattering of X-rays, Wiley, New York, 1955.
[23] O. Glatter, O. Kratky, Small Angle X-ray Scattering, Academic Press, London, 1982.
[24] P.V. Konarev, V.V. Volkov, A.V. Sokolova, M.H.J. Koch, D.I. Svergun, PRIMUS: a Windows PC-based system for small-angle scattering data analysis, J. Appl. Crystallogr. 36 (2003) 1277–1282.
[25] M.V. Petoukhov, P.V. Konarev, A.G. Kikhneya, D.I. Svergun, ATSAS 2.1 – towards automated and web-supported small-angle scattering data analysis, J. Appl. Crystallogr. 40 (2007) s223–s228.
[26] E. Mylonas, D.I. Svergun, Accuracy of molecular mass determination of proteins in solution by small-angle X-ray scattering, J. Appl. Crystallogr. 40 (2007) s245–s249, https://doi.org/10.1107/S1600576715015551.
[27] D.I. Svergun, Determination of the regularization parameter in indirect-transform methods using percentual criteria, J. Appl. Crystallogr. 25 (1992) 495–503.
[28] D.I. Petoukhov, M.V. Svergun, Ambiguity assessment of small-angle scattering curves from monodisperse systems, Acta Crystallogr. Sect. D Biol. Crystallogr. 71 (2015) 1051–1058.
[29] D. Franke, D.I. Svergun, DAMMIF, a program for rapid ab-initio shape determination in small-angle scattering, J. Appl. Crystallogr. 42 (2009) 342–346.
[30] M.B. Kozin, D.I. Svergun, Automated matching of high- and low-resolution structural models, J. Appl. Crystallogr. 34 (2001) 33–41.
[31] V.V. Volkov, D.I. Svergun, Uniqueness of ab initio shape determination in small-angle scattering, J. Appl. Crystallogr. 36 (2003) 860–864.
[32] D.I. Svergun, Restoring low resolution structure of biological macromolecules from solution scattering using simulated annealing, Biophys. J. 76 (1999) 2879–2886.
[33] M.V. Petoukhov, D.I. Svergun, Global rigid body modeling of macromolecular complexes against small-angle scattering data, Biophys. J. 89 (2005) 1237–1250.
[34] T. Nemoto, Y. Ohara-Nemoto, M. Ota, T. Takagi, K. Yokoyama, Mechanism of dimer formation of the 90-kDa heat-shock protein, Eur. J. Biochem. 233 (1995) 1–8.
[35] D. Franke, C.M. Jeffries, D.I. Svergun, Correlation Map, a goodness-of-fit test for one-dimensional X-ray scattering spectra, Nat. Methods 12 (2015) 419–422.
[36] J.G. Nørby, Coupled assay of Na+,K+-ATPase activity, Methods Enzymol. 156 (1988) 116–119. http://www.ncbi.nlm.nih.gov/pubmed/2835597.
[37] M.G.C. Carvalho, M.A. Rebello, Induction of heat shock proteins during the growth of Aedes albopictus cells, Insect Biochem. 17 (1987) 199–206.
[38] R. Zhao, M. Davey, Y.C. Hsu, P. Kaplanek, A. Tong, A.B. Parsons, N. Krogan, G. Cagney, D. Mai, J. Greenblatt, C. Boone, A. Emili, W.A. Houry, Navigating the chaperone network: an integrative map of physical and genetic interactions mediated by the hsp90 chaperone, Cell. 120 (2005) 715–727, https://doi.org/10.1016/j.cell.2004.12.024.
[39] V.C.H. Silva, C.H.I. Ramos, The network interaction of the human cytosolic 90 kDa heat shock protein Hsp90: a target for cancer therapeutics, J. Proteome 75 (2012) 2790–2802, https://doi.org/10.1016/j.jprot.2011.12.028.
[40] S.E. Jackson, Hsp90: structure and function, Top. Curr. Chem. 328 (2013) 155–240, https://doi.org/10.1007/128_2012_356.
[41] C. Prodromou, S.M. Roe, R.O. Brien, J.E. Ladbury, P.W. Piper, L.H. Pearl, Identification and structural characterization of the ATP/ADP-binding site in the Hsp90 molecular chaperone, Cell. 90 (1997) 65–75.
[42] C. Scheufler, A. Brinker, G. Bourenkov, S. Pegoraro, L. Moroder, H. Bartunik, F.U. Hartl, I. Moarefi, Structure of TPR domain–peptide complexes: critical elements in the assembly of the Hsp 70–Hsp90 multichaperone machine, Cell. 101 (2000) 199–210.
[43] K.P. Silva, T.V. Seraphim, J.C. Borges, Structural and functional studies of Leishmania braziliensis Hsp90, Biochim. Biophys. Acta Proteins Proteomics 1834 (2013) 351–361, https://doi.org/10.1016/j.bbapap.2012.08.004.
[44] M.M.U. Ali, S.M. Roe, C.K. Vaughan, P. Meyer, B. Panaretou, P.W. Piper, C. Prodromou, L.H. Pearl, Crystal structure of an Hsp90–nucleotide–p23/Sba1 closed chaperone complex, Nature. 440 (2006) 1013–1017, https://doi.org/10.1038/nature04716.

[45] D.E. Dollins, J.J. Warren, R.M. Immormino, D.T. Gewirth, Structures of GRP94-nucleotide complexes reveal mechanistic differences between the hsp90 chaperones, Mol. Cell 28 (2007) 41–56, https://doi.org/10.1016/j.molcel.2007.08.024.
[46] K.A. Verba, R.Y.-R. Wang, A. Arakawa, Y. Liu, M. Shirouzu, S. Yokoyama, D.A. Agard, Atomic structure of Hsp90-Cdc37-Cdk4 reveals that Hsp90 traps and stabilizes an unfolded kinase, Science (80-.) 352 (2016).
[47] V.C.H. Silva, T.C. Cagliari, T.B. Lima, F.C. Gozzo, C.H.I. Ramos, Conformational and functional studies of a cytosolic 90 kDa heat shock protein Hsp90 from sugarcane, Plant Physiol. Biochem. 68 (2013) 16–22, https://doi.org/10.1016/j.plaphy.2013.03.015.
[48] Y.A. Mendonça, C.H.I. Ramos, Cloning, purification and characterization of a 90 kDa heat shock protein from Citrus sinensis (sweet orange), Plant Physiol. Biochem. 50 (2012) 87–94, https://doi.org/10.1016/j.plaphy.2011.08.001.
[49] P. Csermelys, J. Kajtars, M. Hollosis, G. Jalsovszkyll, S. Hollyv, C.R. Kahnii, P. Gergely, S. Jr, C. Sotis, K. Mihalys, J. Somogyis, ATP induces a conformational change of the 90-kDa heat shock protein (hsp90), J. Biol. Chem. 268 (1993) 1901–1907.
[50] A.K. Shiau, S.F. Harris, D.R. Southworth, D.A. Agard, Structural analysis of *E. coli* hsp90 reveals dramatic nucleotide-dependent conformational rearrangements, 127 (2006) 329–340, https://doi.org/10.1016/j.cell.2006.09.027.
[51] J.C. Borges, C.H.I. Ramos, Analysis of molecular targets of Mycobacterium tuberculosis by analytical ultracentrifugation, Curr. Med. Chem. 18 (2011) 1276–1285.
[52] S.H. McLaughlin, L. Ventouras, B. Lobbezoo, S.E. Jackson, Independent ATPase activity of Hsp90 subunits creates a flexible assembly platform, J. Mol. Biol. 344 (2004) 813–826, https://doi.org/10.1016/j.jmb.2004.09.055.
[53] B.A.L. Owen, W.P. Sullivan, S.J. Felts, D.O. Toft, Regulation of heat shock protein 90 ATPase activity by sequences in the carboxyl terminus, J. Biol. Chem. 277 (2002) 7086–7091, https://doi.org/10.1074/jbc.M111450200.
[54] S.H. Mclaughlin, H.W. Smith, S.E. Jackson, Stimulation of the weak ATPase activity of human Hsp90 by a client protein, J. Mol. Biol. 315 (2002) 787–798, https://doi.org/10.1006/jmbi.2001.5245.
[55] K. Richter, J. Soroka, L. Skalniak, A. Leskovar, M. Hessling, J. Reinstein, J. Buchner, Conserved conformational changes in the ATPase cycle of human Hsp90, J. Biol. Chem. 283 (2008) 17757–17765, https://doi.org/10.1074/jbc.M800540200.
[56] T. Weikl, P. Muschler, K. Richter, T. Veit, J. Reinstein, J. Buchner, C-terminal regions of Hsp90 are important for trapping the nucleotide during the ATPase cycle, J. Mol. Biol. 303 (2000) 583–592, https://doi.org/10.1006/jmbi.2000.4157.
[57] H. Wegele, P. Muschler, M. Bunck, J. Reinstein, J. Buchner, Dissection of the contribution of individual domains to the ATPase mechanism of Hsp90, J. Biol. Chem. 278 (2003) 39303–39310, https://doi.org/10.1074/jbc.M305751200.
[58] C.D. Putnam, Guinier peak analysis for visual and automated inspection of small-angle X-ray scattering data, J. Appl. Crystallogr. 49 (2016) 1412–1419.
[59] T.V. Seraphim, K.P. Silva, P.R. Dores-silva, L.R.S. Barbosa, J.C. Borges, Insights on the structural dynamics of Leishmania braziliensi s Hsp90 molecular chaperone by small angle X-ray scattering, Int. J. Biol. Macromol. 97 (2017) 503–512, https://doi.org/10.1016/j.ijbiomac.2017.01.058.
[60] P. Bron, E. Giudice, J. Rolland, V. Peyrot, D. Thomas, C. Garnier, Apo-Hsp90 coexists in two open conformational states in solution, Biol. Cell. 100 (2008) 413–425, https://doi.org/10.1042/BC20070149.
[61] D. Orthaber, A. Bergmann, O. Glatter, SAXS experiments on absolute scale with Kratky systems using water as a secondary standard, J. Appl. Crystallogr. 33 (2000) 218–225.
[62] N.R. Hajizadeh, D. Franke, C.M. Jeffries, D.I. Svergun, Consensus Bayesian assessment of protein molecular mass from solution X-ray scattering data, Sci. Rep. 8 (2018) 7204.
[63] K.A. Krukenberg, U.M.K. Bottcher, D.R. Southworth, D.A. Agard, Grp94, the endoplasmic reticulum Hsp90, has a similar solution conformation to cytosolic Hsp90 in the absence of nucleotide, Protein Sci. 18 (2009) 1815–1827, https://doi.org/10.1002/pro.191.
[64] A. Giannoulis, A. Feintuch, Y. Barak, H. Mazal, S. Albeck, T. Unger, F. Yang, X. Su, D. Goldfarb, Two closed ATP- and ADP-dependent conformations in yeast Hsp90 chaperone detected by Mn(II) EPR spectroscopic techniques, Proc. Natl. Acad. Sci. U. S. A. 117 (2020) 395–404(LI et al., 2012; PRODROMOU et al., 2000; Giannoulis A, Feintuch A, Barak Y, Mazal H, Albeck S, Unger T, Yang F, Su XC, Goldfarb D).
[65] M. Hessling, K. Richter, J. Buchner, Dissection of the ATP-induced conformational cycle of the molecular chaperone Hsp90, Nat. Struct. Mol. Biol. 16 (2009) 287–293.
[66] C. Graf, C.-T. Lee, L.E. Meier-Andrejszki, M.T.N. Nguyen, M.P. Mayer, Differences in conformational dynamics within the Hsp90 chaperone family reveal mechanistic insights, Front. Mol. Biosci. 1 (2014) 4, https://doi.org/10.3389/fmolb.2014.00004.
[67] S. Tsutsumi, M. Mollapour, C. Prodromou, C. Lee, B. Panaretou, S. Yoshida, M.M. Mayer, L.M. Neckers, Charged linker sequence modulates eukaryotic heat shock protein 90 (Hsp90) chaperone activity, Proc. Natl. Acad. Sci. U. S. A. 109 (2012) 2937–2942, https://doi.org/10.1073/pnas.1114414109.
[68] M. Jahn, A. Rehn, B. Pelz, B. Hellenkamp, K. Richter, M. Rief, J. Buchner, T. Hugel, The charged linker of the molecular chaperone Hsp90 modulates domain contacts and biological function, PNAS. 111 (2014) 17881–17886.
[69] S. Tsutsumi, M. Mollapour, C. Graf, C.-T. Lee, B.T. Scroggins, W. Xu, L. Haslerova, M. Hessling, A.A. Konstantinova, J.B. Trepel, B. Panaretou, J. Buchner, M.P. Mayer, C. Prodromou, L. Neckers, Hsp90 charged-linker truncation reverses the functional consequences of weakened hydrophobic contacts in the N domain, Nat. Struct. Mol. Biol. 16 (2009) 1141–1147.
[70] G.E. Dale, C. Oefner, A. D'Arcy, The protein as a variable in protein crystallization, J. Struct. Biol. 142 (2003) 88–97, https://doi.org/10.1016/S1047-8477(03)00041-8.
[71] A. Sivan, A.N. Shriram, N. Muruganandam, R. Thamizhmani, Expression of heat shock proteins (HSPs) in Aedes aegypti (L) and Aedes albopictus (Skuse) (Diptera: Culicidae) larvae in response to thermal stress, Acta Trop. 167 (2017) 121–127.
[72] L. Zhao, J.J. Becnel, G.G. Clark, K.J. Linthicum, Expression of AeaHsp26 and AeaHsp83 in Aedes aegypti (Diptera: Culicidae) larvae and pupae in response to heat shock stress, J. Med. Entomol. 47 (2010) 367–375, https://doi.org/10.1603/ME09232.
[73] E.J. Muturi, A. Nyakeriga, M. Blackshear, Temperature-mediated differential expression of immune and stress-related genes in Aedes aegypti larvae, J. Am. Mosq. Control Assoc. 28 (2012) 79–83.
[74] M.G.C. Carvalho, M.S. Freitas, Effect of continuous heat stress on cell growth and protein synthesis in Aedes albopictus, J. Cell. Physiol. 137 (1988) 455–461.